ENVIRONMENTAL RESEARCH
LETTERS

PURPOSE-LED PUBLISHING™ Part of the ENVIRONMENTAL RESEARCH SERIES

LETTER • **OPEN ACCESS**

Exploring the bounds of methane catalysis in the context of atmospheric methane removal

To cite this article: Aliki Marina Tsopelakou *et al* 2024 *Environ. Res. Lett.* **19** 054020

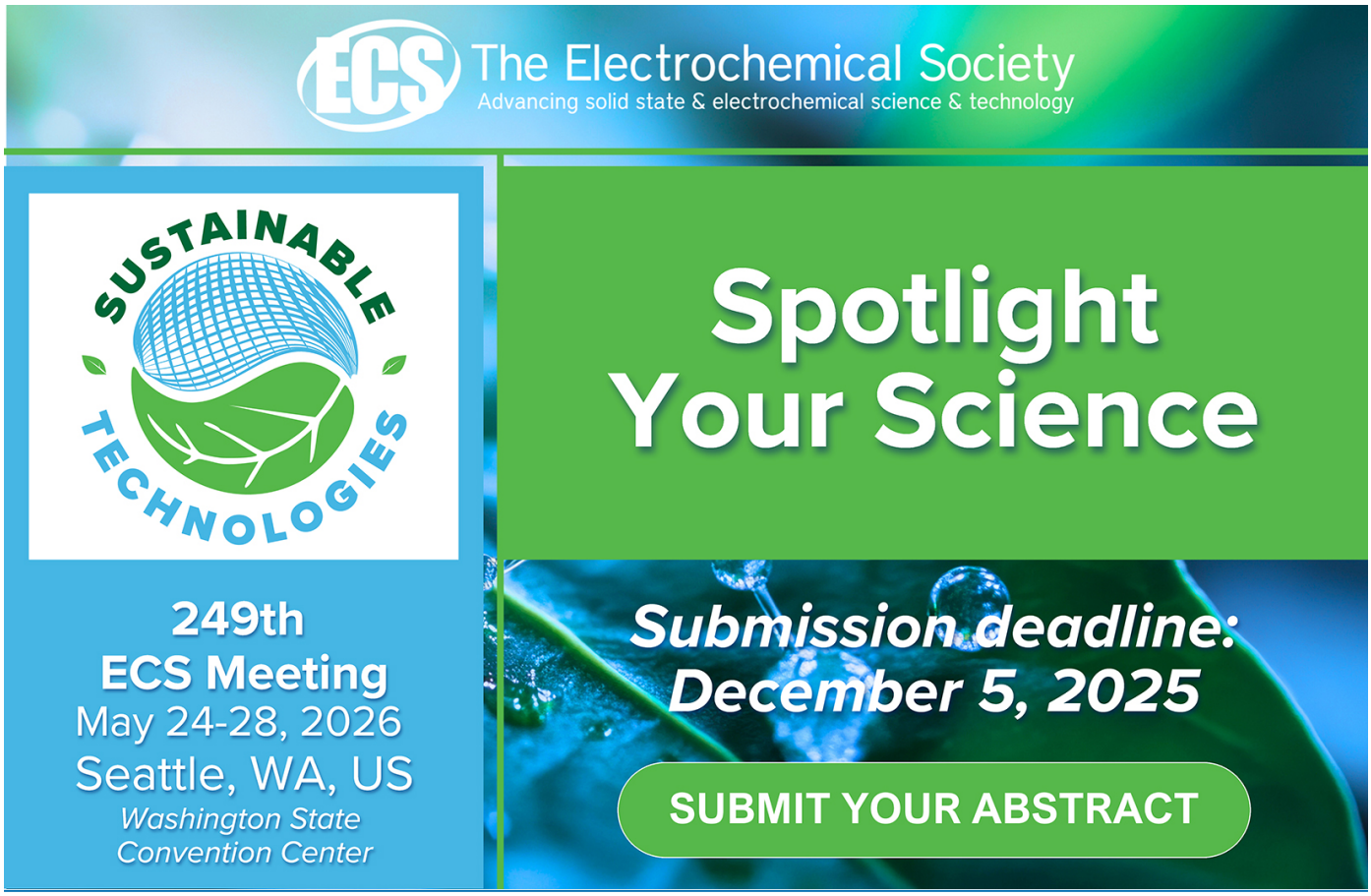

IOP Publishing Environ. Res. Lett. 19 (2024) 054020 https://doi.org/10.1088/1748-9326/ad383f

ENVIRONMENTAL RESEARCH
LETTERS

OPEN ACCESS

RECEIVED
31 October 2023

REVISED
19 February 2024

ACCEPTED FOR PUBLICATION
27 March 2024

PUBLISHED
16 April 2024

LETTER

Exploring the bounds of methane catalysis in the context of atmospheric methane removal

Aliki Marina Tsopelakou[1,2], **Joe Stallard**[1], **Alexander T Archibald**[3,4], **Shaun Fitzgerald**[1,2] and **Adam M Boies**[1,2,*]

[1] Department of Engineering, University of Cambridge, Cambridge, United Kingdom
[2] Centre for Climate Repair, Cambridge, United Kingdom
[3] Yusuf Hamied Department of Chemistry, University of Cambridge, Cambridge, United Kingdom
[4] National Centre for Atmospheric Science, University of Cambridge, Cambridge, United Kingdom
[*] Author to whom any correspondence should be addressed.

E-mail: amb233@cam.ac.uk

Keywords: atmospheric methane removal, catalytic technologies, forced convection, energy requirements analysis

Supplementary material for this article is available online

Abstract

Methane, a potent greenhouse gas, is a significant contributor to global warming, with future increases in its abundance potentially leading to an increase of more than 1°C by 2050 beyond other greenhouse gases if left unaddressed. To remain within the crucial target of limiting global warming to 1.5 °C, it is imperative to evaluate the potential of methane removal techniques. This study presents a scoping analysis of different catalytic technologies (thermal, photochemical and electrochemical) and materials to evaluate potential limitations and energy requirements. An analysis of mass transport and reaction rates is conducted for atmospheric methane conversion system configurations. For the vast majority of catalytic technologies, the reaction rates limit the conversion which motivates future efforts for catalyst development. An analysis of energy requirements for atmospheric methane conversion shows minimum energy configurations for various catalytic technologies within classic tube or parallel plate architectures that have analogs to ventilation and industrial fins. Methane concentrations ranging from 2 ppm (ambient) to 1000 ppm (sources, such as wetlands, fossil-fuel extraction sites, landfills etc) are examined. The study finds that electrocatalysis offers the most energy efficient approach (∼0.2 GJ tonne^{-1} CO_2e) for new installations in turbulent ducts, with a total energy intensity <1 GJ tonne^{-1} CO_2e. Photocatalytic methane removal catalysts are moderately more energy intensive (∼2 GJ tonne^{-1} CO_2e), but could derive much of their energy input from 'free' solar energy sources. Thermal systems are shown to be excessively energy intensive (>100 GJ tonne^{-1}), while combining photovoltaics with electrochemical catalysts (∼1 GJ tonne^{-1} CO_2e) have comparable energy intensity to photocatalytic methane removal catalysts.

1. Introduction

Methane is the fastest growing greenhouse gas (GHG) and has approximately 80.8–82.5 (natural, fossil, respectively) times the global warming potential of carbon dioxide over a 20 year time-span [1]. A commitment to reduce methane emissions was made by 111 countries subsequent to the COP26 summit, with a reduction target of 30% by 2030. This commitment has initiated growth of emissions abatement and methane removal technologies. Studies have estimated that current technologies can achieve significant methane emissions reductions (∼50%), but there remains a need for more approaches that enable ambient methane removal [2]. Methane is released from a wide variety of agricultural, industrial, and natural sources, making its abatement quite challenging. The oil and gas industry, contributing to around 30% of total emissions, could primarily eliminate leaks and off gassing by implementing monitoring programs rather than relying on catalysis. Conversely, a significant and increasing fraction of methane, around 40%, comes from wetlands and other natural sources, and about 39% from farming.

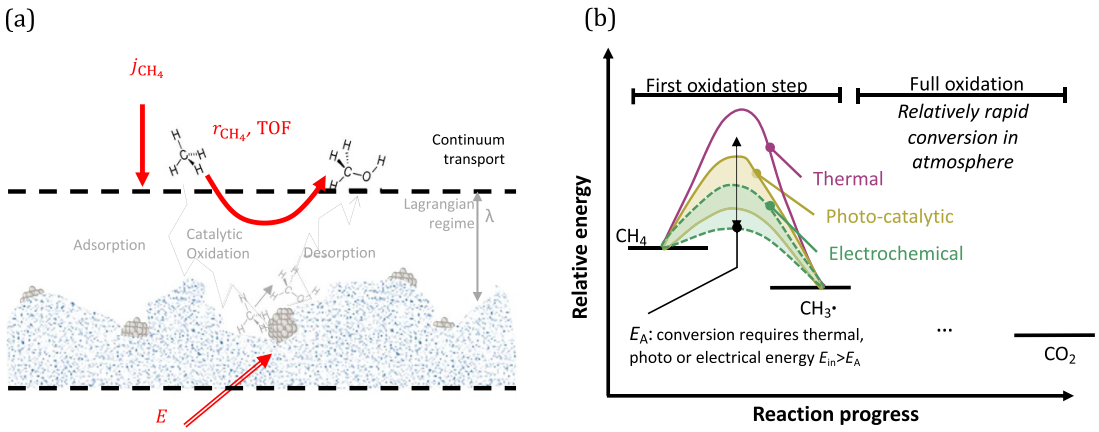

Figure 1. (a) Schematic representation of methane catalysis technologies, including bulk flux of methane, (j_{CH4}), reaction rates, (r_{CH_4}), turn over frequency, (ν_{TOF}), energy (E). Further processes shown in grey that are not reported in all literature include adsorption, oxidation processes, desorption and Lagrangian transport processes. The black dashed lines bound our system. (b) Reaction pathways indicating activation energy required for catalyst strategies.

These emissions are more difficult to control through leak detection and mitigation [3].

Reducing methane emissions and extracting methane from the atmosphere may both contribute to lowering the concentration of atmospheric methane. One methane abatement method that has been proposed, based on natural analogues [4], is the use of Cl radicals in air. According to models, such an approach would effectively remove methane and may also reduce harmful tropospheric ozone air pollution [5]. Jackson *et al* [6] reported that removing approximately three years' worth of human-caused methane emissions could decrease global warming by 0.21 °C. Zosia *et al* [7] showed that removing all anthropogenic methane emissions from 2020 would result in not only 1 °C reduction in surface temperature, but air quality improvements that would lead to a reduction of 690 000 premature deaths per year by 2050. The temporary temperature effect of removing one year's worth of human-caused methane emissions would be roughly four times greater than that of removing the equivalent amount of carbon dioxide emissions. The main technological pathways for removing methane are the application of catalytic chemical oxidation (thermal, photochemical, electrochemical), the enhancement of atmospheric sinks, and the conversion of methane using microbes [6, 8, 9]. Herein, we focus on methane conversion by means of thermal, photochemical and electrochemical catalysis.

The challenge for atmospheric methane is that although oxidation releases energy, the energy release is insufficient to sustain a reaction. The methane C–H bond is strong, requiring 439 kJ mol^{-1} to break [10], but in the presence of oxygen results in an exothermic release of 890 kJ mol^{-1} for fully oxidized products. However, the enthalpy of oxidation for 100 ppm in air of CH_4 increases the kinetic energy of the gas by only ∼1%, which is insignificant at diluted concentrations, resulting in a ∼3 K temperature increase in the surrounding gas. Thus, a primary constraint in implementing large-scale methane conversion is providing the energy to overcome the activation energy for successive methane oxidation reactions. Heterogeneous catalysts offer the potential to lower the activation energy, by means of providing a surface that adsorbs, converts and releases the methane molecule and its product(s).

The viability of heterogeneous catalyst technologies for methane oxidation depends on a variety of factors, such as rates of reaction, required energy inputs, mass transport to the catalyst surface, cost of implementation, technology longevity etc. To evaluate the potential for heterogeneous catalyst approaches to atmospheric methane oxidation, it is useful to explore fundamental limits, such as mass transfer to surfaces, as well as catalyst activation energies to bound the potential for such approaches. Therefore, our purpose is to explore catalytic rates (e.g. activities, turn over frequencies and limitations) to mass transport in classical engineered configurations for a variety of heterogeneous catalytic approaches. Our objective is to evaluate the potential for methane conversion technologies employed in thermal, electrochemical and photochemical processes.

Figure 1(a) presents the macroscopic descriptors of heterogeneous catalyst technologies of interest herein: mass flux to the surface (j_{CH4}), reaction rate (r_{CH_4}), turn-over frequency (ν_{TOF}) and activation energy (E_a). These processes are dictated by microscale processes such as adsorption, catalytic oxidation, desorption and Lagrangian regime (grey) that most studies do not report. In particular, adsorption and desorption rates are dictated by binding energies, often depicted in volcano plots [11, 12], and

play a critical role in catalyst performance per the Sabatier Principle [13]. However binding energies, as well as other properties (e.g. pore sizes and surface structure), are not consistently reported in literature. As our purpose is to investigate the viability of methane catalysis across a range of technologies, we have homogenized the range of results commonly reported in literature into the parameters indicated by red arrows crossing the system bounds (dashed black lines).

1.1. Methane catalysis

In the context of this work, methane heterogeneous catalysts are considered that increase the oxidation state of the methane molecules through chemical reactions facilitated at material surfaces. Thus, the partial oxidation of methane may result in methanol (CH_3OH), formaldehyde (CH_2O), or other oxygenated compounds. Another research focus lies in heterogeneous catalysis aimed at generating reactant species for subsequent gas-phase reactions with methane, such as chlorine [14]. As an example the Methane Eradication Photochemical System relies on gas-phase radicals for methane degradation [15] and is not subject to surface rate limitations. While those approaches exhibit promise and are poised for further development, our study considers solely heterogeneous catalysis for direct surface conversion of methane.

Normally, thermo-catalytic methane oxidation requires high reaction temperatures ($>300\,^{\circ}C$) to occur, where platinum group metals (PGMs), e.g. Pt, Pd and Rh, have proved the most efficient catalysts. However, some transition metal oxides e.g. CuO, V_2O_5, TiO_2 have also been used as methane oxidation catalysts, due to their lower cost.

Catalytic processes that operate at low temperatures, such as photocatalysis, electrocatalysis, and photoelectrocatalysis, have been developed to promote reactions under mild conditions. These methods serve as alternatives to traditional thermocatalysis, which requires high temperatures. The most common photocatalysts applied are TiO_2 [16, 17] and ZnO [18, 19] offering a potential low-temperature route to achieve methane conversion. The efficiency of photocatalysts is known to change with temperature and humidity. Some approaches are only effective at completely dry conditions or for relative humidities less than 5% [20], and thus their application to ambient methane removal is not plausible. While there is promise in the early laboratory results, there remains significant challenges in progressing to higher technology readiness levels.

The potential integration of catalytic methane conversion into diverse contexts is being explored as a means to facilitate *in−situ* mitigation of methane and reduce emissions. Methane catalysts are available for compressed natural gas vehicles and are being explored for applications in the ventilation infrastructure of coal mines and gas fields, as well as domestic heating systems.

1.2. Thermal, electrical and photocatalysis

To enhance the reaction rate at low methane concentrations in thermal catalysis, strategies need to be implemented to reduce the activation energy while maintaining a constant temperature. The turn-over frequencies (TOFs), activation energies, temperature, reactant concentrations, catalyst surface area and stoichiometry of the reaction are typically required in order to determine the reaction rates for catalyst technologies. Data from all known studies on thermal gas-phase methane oxidation have been collected and presented in section 3 for different metals and substrates enabling for direct methane reaction rate comparisons.

Photocatalytic processes involve the use of a photocatalyst to initiate chemical reactions under light irradiation. Photocatalysts are typically semiconducting materials that can absorb light energy and generate electron–hole pairs. These materials can facilitate methane conversion by activating methane molecules under light irradiation and are often paired with PGMs. Direct cleavage of the C–H bond ($\sim$415 kJ mol^{-1}) [10] requires photon energies in the UV range ($\lambda < 300$ nm), thus guiding the selection of semiconducting materials. The current leading photocatalyst material is Ag @ZnO with 8% quantum yield at wavelengths < 400 nm [18]. Photocatalytic reactions can induce reactions to proceed at lower (or room) temperatures. This capability offers several benefits, including reduced energy consumption and the preservation of catalyst stability. Herein, photocatalytic data has been surveyed from all known academic methane sources also shown in section 3.

Electrocatalysts facilitate redox reactions, where electrons are transferred between the reactants. In these reactions, the electron charge (e^-) is transferred between the catalyst and the reacting species. The catalytic sites often have tailored electronic configurations that allow methane adsorbtion and are typically metals or metal oxides. The primary engineering parameters that govern electrochemical catalysis are current (charge transfer rate), voltage (oxidation potential), electrode area (adsorption sites) as well as temperature, methane concentration, and loading among others.

Table 1 presents catalytic methods for extracting methane from the atmosphere. While thermal catalysis is energy-intensive and requires controlled heating environments, it can still find applications in specific internal scenarios, especially within ducting systems. Photochemical catalysis primarily relies on external light sources, while UV light can be applied internally, e.g. inside ducts. Electrocatalysis shows promise for internal applications due to its energy efficiency and versatility.

Table 1. Summary table of catalytic methods for extracting methane from atmosphere. Internal applications pertain to utilization within ducting systems where convective flow occurs, whereas external applications involve surfaces exposed to the environment, such as building surfaces. Internal application of photocatalysis is achievable solely through UV light exposure.

Catalytic methods	Energy source	Application
Thermal catalysis	Chemical conversion, waste heat	Internal
Photocatalysis	Solar or UV light	External
Electrocatalysis	Electricity (renewable or conventional)	Internal

Figure 1(b) provides a conceptual illustration of the activation energy required for catalyst strategies, for the first oxidation step from methane conversion to methanol. The heats of formation for CH_4, CH_3 and CO_2, are -74.8 kJ mol^{-1}, 145.7 kJ mol^{-1} and -393.5 kJ mol^{-1} [10], respectively. In thermal catalysis, the activation energy, E_a, required is generally higher than that in photocatalysis and electrocatalysis. As is shown, this observation underscores the potential advantages of photocatalytic and electrocatalytic processes, as they may enable more energy-efficient pathways for catalytic reactions.

Well-designed catalyst systems often provide molecular fluxes in excess of the catalytic rate when mass transport is 'cheap' relative to the catalyst 'cost'. More specifically, to maximize the cost-effectiveness of system components, it is essential to employ well-optimized processes that ensure an abundant supply of the more economical component. For instance, in situations where mass transport is economically favorable compared to catalyst cost, the molecular flux to surfaces will exceed the conversion rate, resulting in catalytically rate-limited processes. Here we may consider 'cost' in either energy, carbon intensity or financial terms. To facilitate comparisons of molecular fluxes to molecular conversion, reaction data was compiled from a variety of different methane conversion technologies. Reaction rate information appears in a variety of reported values in literature including TOFs and molar conversion per projected surface area, catalyst surface area and catalyst mass with assumed first and second order reactions (see tables SI1–3 and figures SI1–6). We have homogenized this data to comply with the first order reaction rate equation with respect to methane concentration, as shown in equation (1).

$$R = [CH_4]\ k\, e^{-E_a/(R\,T)} \qquad \left[\text{mol s}^{-1}\ \text{m}^{-2}\right]. \quad (1)$$

For thermal systems, data related to catalyst and support materials, reaction temperature, metal loading (often PGMs), dispersion, TOFs, activation energies, etc have been classified for different methods of methane conversion (e.g. oxidation, steam reforming) allowing for the final evaluation of the thermal reaction rates. For photochemical systems additional data such as power, light intensity, wavelength, and photoirradiated area have been gathered. Similarly, the voltage, current and electrode area have been extracted from different electrocatalytic reactions and studies for the calculation of the corresponding reaction rates. Raw data on reaction rates were provided for the various studies enabling a direct evaluation (tables SI1–3). While the vast majority of thermocatalytic studies [21–26] report reaction rates per catalyst support surface area, here we normalize results per projected area.

2. Mass transport formulation

The mass transport of gas molecules towards reaction sites occurs at two length scales; firstly via the bulk transport of fluid to the vicinity of the solid interface, and secondly via molecular diffusion within the boundary layer at the interface. The former depends on the fluid embodiment of the system while the latter on the composition of the gas-phase, and surface structure.

Mass transport limitations related to a disconnect in catalyst performance evaluation can be overcome via the use of gas diffusion electrode (GDE) technology [27]. This technology involves the use of specialized electrodes designed with a porous structure to enhance the mass transport of gases, e.g. methane, to the electrochemical reaction sites. The GDE innovation ensures improved contact between the reactant and the catalyst, overcoming concerns about the effectiveness of electrocatalysis in low-solubility scenarios [27, 28].

Testing systems (e.g. ducts, monoliths and parallel plates) can accommodate thermal, electrical and/or photochemical reactions in realistic fluid geometries and flow regimes, which reflect use cases of proposed catalytic systems. In order to compare methane conversion rates to surface fluxes, we evaluate mass transport of atmospheric-level methane at a gas-solid interface, for realistic flow geometries and conditions. This enables us to provide a framework for evaluating the mass transport energy and material intensity of emerging methane abatement technologies.

2.1. Forced convective flow over parallel flat plates and ducts

In forced convection, fluid movement is induced by an external pressure source (e.g fan) to overcome the pressure drop caused by viscous dissipation of energy because of stationary walls. Figure 2 illustrates the mass transport in laminar and turbulent flow as characterized by the Reynolds number $Re = \rho V d/\mu$ for parallel flat plates and ducts for a given density ρ, velocity V and viscosity μ. Both configurations have been examined, while the calculated rate of mass

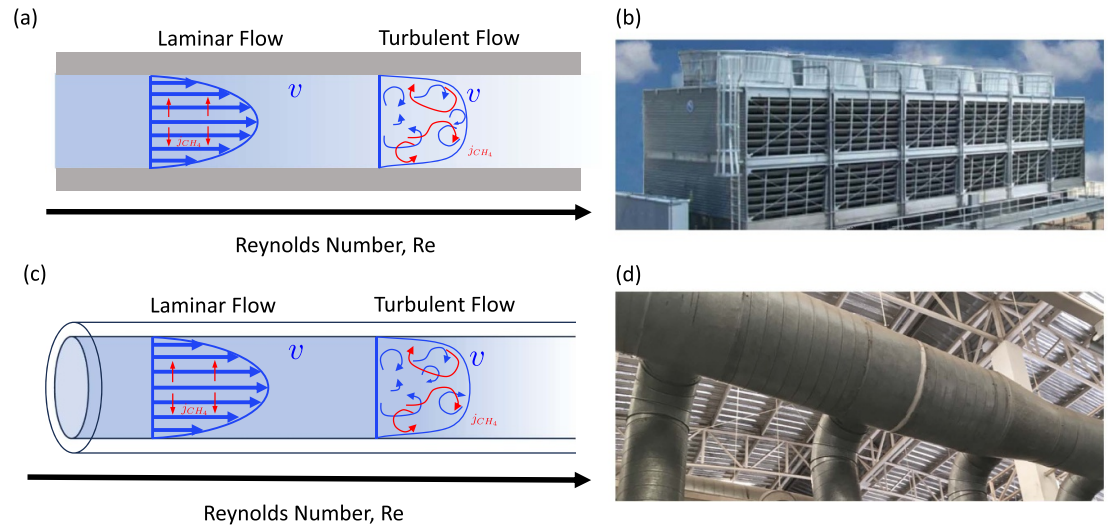

Figure 2. Mass transport over parallel flat plates (a)–(b) and ducts (c)–(d) at laminar and turbulent flows.

transfer (i.e. molecular flux) is influenced by the flow conditions (laminar or turbulent), the properties of the multicomponent fluid (e.g. diffusivity of methane in air), and the geometry of the system (e.g. diameter of the duct, gap thickness of parallel flat plates).

Mass transfer rates are known solutions for these configurations and can be expressed as the dimensionless ratio of convective mass diffusion h_m and characteristic diameter d to mass diffusivity D known as the Sherwood number $Sh = h_m d/D$. The Sherwood relation can be found as a function of Schmidt number Sc,

$$Sh = 0.332 \cdot Sc^{1/3} \cdot Re^{1/2}, \tag{2}$$

where $Sc = \nu/D$ is the ratio of kinematic viscosity ν to the diffusivity of methane at given temperatures. The Sherwood number for parallel flat plates in the turbulent regime is given by

$$Sh = 0.037 \cdot Sc^{1/3} \cdot Re^{4/5}. \tag{3}$$

The Sherwood expressions for a duct in laminar and turbulent flow, are described via equations (4) and (5), respectively.

$$Sh = 3.13, \tag{4}$$

$$Sh = 0.023 \cdot Sc^{1/3} \cdot Re^{4/5}. \tag{5}$$

The molecular flux, j, can be evaluated via the Sherwood numbers obtained from the above expressions, for the different configurations at varying methane concentration (C at 2 ppm, 100 ppm, 1000 ppm) and plate gap thicknesses t or duct diameters d according to equation (6). By evaluating the integral from 0 to d or t, the corresponding molecular fluxes are given as,

$$j\,(T) = \frac{Sh \cdot D \cdot C}{d} \quad \text{or} \quad j\,(T) = \frac{Sh \cdot D \cdot C}{t} \quad \left[\frac{\text{mol} \cdot \text{m}^2}{\text{s}}\right]. \tag{6}$$

The length of the ducts is evaluated (see equation (13), SI) as an exponential expression considering an optimal conversion rate at 63%. A higher conversion rate at 99% has been also examined (see figure 10, SI) resulting in diminishing returns of longer piping, and thus higher energy requirements. Further analytical development is provided in the supplementary information (SI).

3. Catalyst properties

Figure 3 shows thermo-catalytic reaction rates (solid symbols) ranging from 10^{-13}–10^{-4} mol $(\text{m}^2 \cdot \text{s})^{-1}$ where there is no discernible trend across tested temperatures. Molecular fluxes to the projected surface areas (10^{-5}–10^{6} mol $(\text{m}^2 \cdot \text{s})^{-1}$) are typically orders of magnitudes higher than catalyst conversion rates thus indicating most configurations will be reaction-rate limited. All turbulent configurations provide fluxes >9 orders of magnitude greater than the molecular reaction rate of thermal catalysts. The molecular fluxes depend on the methane concentration where atmospheric levels of methane at 2 ppm ($\sim 10^{-5}$ mol $(\text{m}^2 \cdot \text{s})^{-1}$) have proportionally lower fluxes than 100 ppm ($\sim 10^{-3}$ mol $(\text{m}^2 \cdot \text{s})^{-1}$) and 1000 ppm ($\sim 10^{-2}$ mol $(\text{m}^2 \cdot \text{s})^{-1}$) for laminar ducts. In only the laminar duct configuration do a few catalyst molecular rates exceed the molecular fluxes at

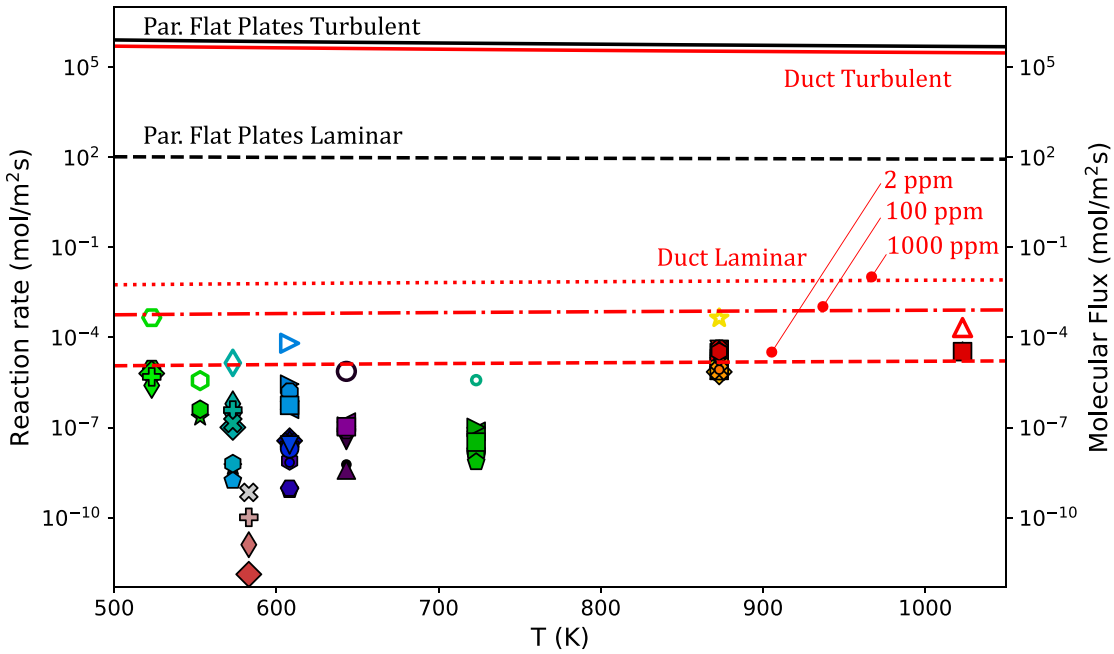

Figure 3. Reaction rates and molecular fluxes against temperature in thermal catalytic systems. The molecular fluxes for the different configurations are calculated at 2 ppm. The duct laminar configuration is also evaluated for 100 ppm and 1000 ppm (further details in SI figure 1) [16, 19, 21–26, 29–43].

the lower methane concentrations of 2 ppm, indicating rare instances of transport limited kinetics [21, 22, 26]. The empty (unfilled) symbols correspond to reaction rates expressed in terms of catalytic area to show an extreme upper bound of catalyst loading where the entire surface is covered with the active materials, e.g. PGMs, where the reaction rates approach the laminar duct configuration molecular flux at 100 ppm. In all other instances the molecular fluxes vastly exceed the reaction rates.

Examining the best performing thermal catalysts provides insights for engineered material approaches. Pd-Ni over halloysite nanotube support (Hal) operating at 523 K achieved a rate of 9.3 $\cdot 10^{-6}$ mol $(m^2 \cdot s)^{-1}$ [26]. High methane conversion is also observed for Pd-Co/Hal and Pd/Hal at 523 K, with reaction rates of 6.3 $\cdot 10^{-6}$ mol $(m^2 \cdot s)^{-1}$ and 4.9 $\cdot 10^{-6}$ mol $(m^2 \cdot s)^{-1}$, respectively [26], as well as for Pd/Al_2O_3 [21] with 2.8 $\cdot 10^{-6}$ mol $(m^2 \cdot s)^{-1}$. Although higher rate catalysts (e.g. Ru/Al_2O_3 and Ru/ZrO_2 at 4.3 $\cdot 10^{-5}$ mol $(m^2 \cdot s)^{-1}$ and 3.5 $\cdot 10^{-5}$ mol $(m^2 \cdot s)^{-1}$ [22]) are also presented in figure 3, they require an operation temperature over 873 K which is outside the interest of the current work. A recent study [29] shows that biomimetic copper zeolite can effectively convert atmospheric and low-level methane (2–20 000 ppm) at relatively low temperatures (473–573 K) under simulated air conditions.

Photocatalytic methane conversion is shown in figure 4 with reaction rates ranging from 10^{-9} to 10^{-3} mol $(m^2 \cdot s)^{-1}$. The photocatalysts are grouped based on the spectral range of light used (e.g. UV, visible) and there is a positive correlation between rate and light intensity. Higher intensities ($\geqslant 10^3$ W m^{-2}) have often been tested for the visible and solar spectrums, where air mass (AM) 1.5G sunlight corresponds to 1000 W m^{-2}. The Pt/TiO_2 [16] material, operating with solar spectrum (AM 1.5G), has the highest measured reaction rate (3.4 $\cdot 10^{-4}$ mol $(m^2 \cdot s)^{-1}$). This rate is higher than the molecular flux at low laminar concentrations (2 and 100 ppm). However, all photocatalysts experiments in literature are tested at high methane concentrations, and almost none of them are for less than 1000 ppm. Similar to thermal catalysts, all configurations except laminar ducts are severely reaction rate limited, indicating that methane conversion systems will benefit from enhanced catalytic rates. Nonetheless, photocatalysts operating in the visible and solar spectrum achieve reasonably high rates ($>10^{-2}$ mol $(m^2 \cdot s)^{-1}$) and offer the potential to minimize the operational energy requirements using a 'free' energy source for methane decomposition.

The electrocatalytic methane systems are shown in figure 5 where molecular conversion rates are depicted versus input power densities for a range of applied voltages (groupings). The electrocatalytic systems achieve higher reaction rates (10^{-7}–10^{-1} mol $(m^2 \cdot s)^{-1}$) than the photocatalytic and thermocatalytic systems. However, many of the measured rates in literature were also tested at elevated temperatures, thus combining effects of thermal and electrocatalysis. While quantum chemistry indicates that

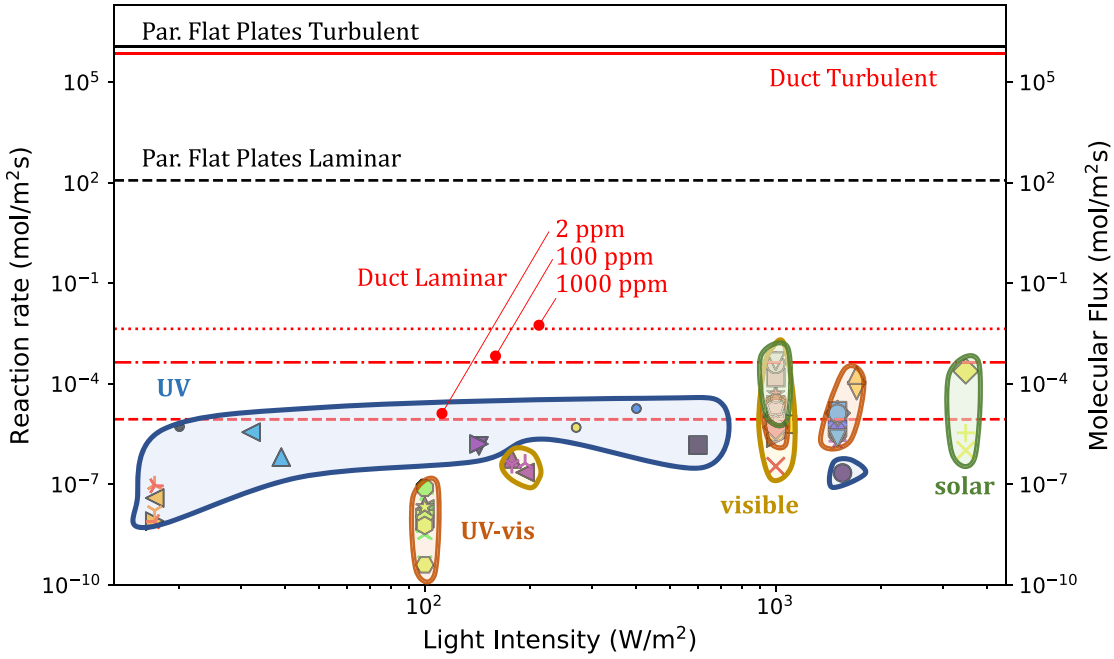

Figure 4. Reaction rates and molecular fluxes against light intensity in photocatalytic systems. The molecular fluxes for the different configurations are calculated at 2 ppm. The duct laminar configuration is also evaluated for 100 ppm and 1000 ppm (further details in SI figure 3) [16, 19, 30–37].

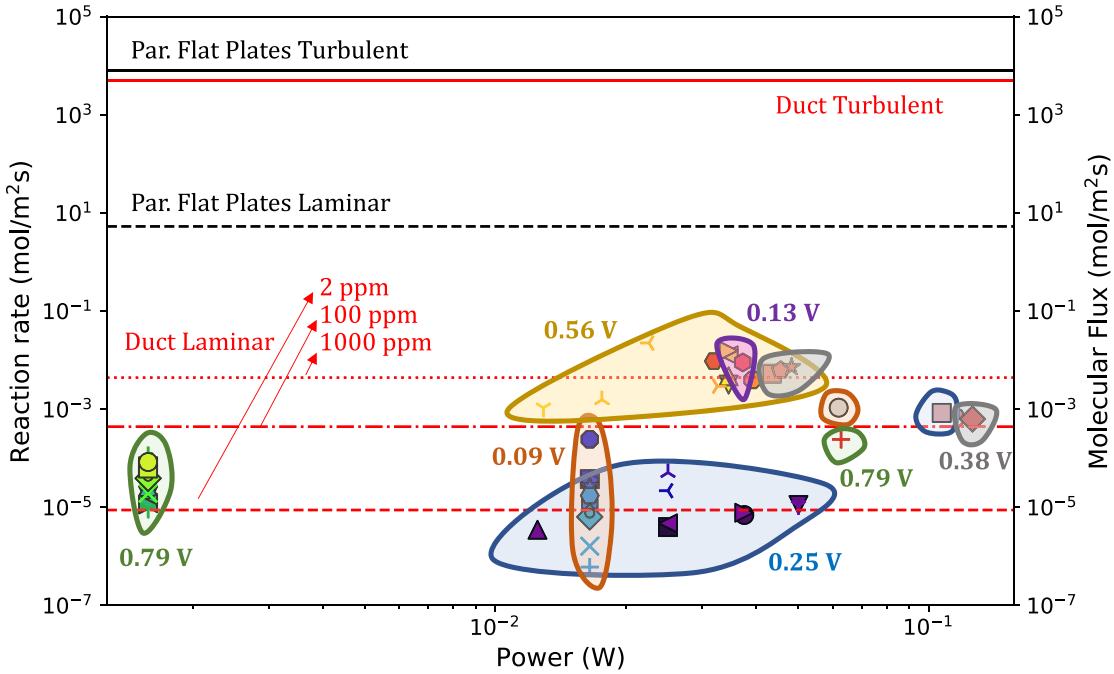

Figure 5. Reaction rates and molecular fluxes as a function of power density in electrocatalytic systems. The molecular fluxes for the different configurations are calculated at 2 ppm. The duct laminar configuration is also evaluated for 100 ppm and 1000 ppm (further details in SI figure 5) [38–43].

individual molecular reactions require input energies that exceed a threshold activation, there appears to be no consistent trend between rates and applied voltages as may be obscured by different testing temperatures. The upper bound of electrocatalytic reaction rates is ∼2 orders of magnitude higher than solely photocatalytic or thermal systems. However, the majority of configurations are still reaction rate limited and would benefit from further catalyst improvements. The V_2O_5/SnO_2 [38] electrochemical catalyst operating at 373 K achieves a reaction rate of 10^{-4} mol $(m^2 \cdot s)^{-1}$ at 0.79 V and 32 W m^{-2} and is the highest rate of those tested near ambient temperatures. Although higher reaction rates have

been measured [41], they were tested at high reaction temperatures (1073 K) that are not viable for large-scale methane removal. The typical methane concentrations of electrocatalytic experiments in literature are $\geqslant 10^5$ ppm [38, 40–43]. Currently, ambient temperature electrocatalysts have comparable (but lower) rates than photocatalysts which would benefit from further development as increased rates could be readily matched with sufficient molecular fluxes.

4. Estimation of energy requirements

The central task of this work is to determine whether atmospheric methane removal has any viability at scale and provide insights into potential technologies. Thus, estimations of methane removal energy requirements (figure 6) are assessed for the different catalytic technologies in forced convection technologies with catalysts applied to various ducting configurations, i.e. representative of monoliths, piping or ventilation. The first order energy considerations indicate that a target of <1 GJ tonne^{-1} CO_2e may be possible when considering first order contributions of convection energy E_{conv} (energy to move air), the capital energy E_{cap} (energy intensity of bulk materials), and the input energy for the different types of catalysts, i.e. thermal $E_{Thermal}$, photochemical E_{Photo} and electrochemical E_{Elec}. The representative assessment is made for fixed convection ($Re = 1.7{\cdot}10^5$), indicative of standard ventilation ducts in turbulent flow with a variety of duct diameters (~5 mm to 1 m, see SI for *Re* variation and further analyses).

The required scale of airflow and number of units depends on air methane concentrations, thus E_{conv} and E_{cap} are evaluated at 2 ppm, 100 ppm and 1000 ppm. E_{cap} is the sum of the ducting structure, $E_{structure}$, considering representative metals, e.g. ducting aluminium (200 MJ kg^{-1}) [44] and steel (20 MJ kg^{-1}) [45] and catalyst energy, $E_{cat,\,cap}$ intensities (further details in SI section 4).

The energy intensity for methane removal normalized to CO_2 (GJ tonne^{-1} CO_2e) for a 20 year time horizon ($GWP20_{CH4} = 86$) [1] and annual energy requirement for each technology are evaluated for the best currently available catalyst system scaled to removal rates of anthropogenic annual methane emissions (0.36 Gt CH_4 yr^{-1}) [6] at current methane concentrations (~2 ppm). The 20 years GWP is mainly considered allowing for a more immediate response to the climate effects of methane emissions. However, the results are also evaluated for 100 years GWP ($GWP100_{CH4} = 34$). Thermal catalysts had an energy intensity of $E_{Thermal}$ ~180 GJ tonne^{-1} CO_2e (455 GJ tonne^{-1} CO_2e GWP100) , where the energy required for the required mass of air is calculated by $E_{Thermal} = m_{air} \cdot C_p \cdot \Delta T$. Recycled heat is considered for incoming/outgoing air heat exchange at an efficiency of $\eta \sim 0.9$. The calculated photocatalytic energy intensity was E_{Photo} ~2 GJ tonne^{-1} CO_2e (5 GJ tonne^{-1} CO_2e GWP100) as evaluated for a Pt/TiO_2 [16] system exposed to the solar spectrum (1000 W m^{-2}). Electrocatalytic systems had the lowest energy intensities at $E_{Elec} = 0.2$ GJ tonne^{-1} CO_2e (0.5 GJ tonne^{-1} CO_2e GWP100) as determined for V_2O_5/SnO_2 [38] (see figure 5) at measured powers (product of reported current and voltage) [38]. The V_2O_5/SnO_2 [38] catalyst is selected as the optimal choice among the other catalysts shown in figure 5 where a temperature of 373 K is applied.

Figure 6 shows that the estimated methane removal energy intensity (left *y*-axis) achieves a minimum when the convective E_{conv} and material capital E_{cap} are balanced (red circle) at ~0.15 GJ tonne^{-1} CO_2e (0.38 GJ tonne^{-1} CO_2e GWP100). The equivalence E_{conv} and E_{cap} occurs for a duct diameter of $d =$ 0.17 m, corresponding to individual volumetric flow rate, $V_i = 0.35$ m^3 s^{-1} (equation (15), SI) which balances the increased convective energy due to pressure drop at small diameters with increased mass transport to the catalyzed walls. Critically, at this optimum E_{conv} and E_{cap} have energy intensities comparable to electrocatalytic intensities E_{Elec} ~0.15 GJ tonne^{-1} CO_2e (0.38 GJ tonne^{-1} CO_2e GWP100).

These results suggest that electrocatalytic coatings paired with an optimal forced-flow ducting configuration could result in a total energy intensity <1 GJ tonne^{-1} CO_2e as $E_{tot} = E_{cap} + E_{conv} + E_{Elec} \approx 0.5$ GJ tonne^{-1} CO_2e (1.26 GJ tonne^{-1} CO_2e GWP100). The resulting total energy required for removal of all annual anthropogenic methane emissions (right *y*-axis) would be of the order ~ 10^{10} GJ yr^{-1} which represents ~2% of the total world energy production (~$6{\cdot}10^{11}$ GJ yr^{-1}) [46]. Conversely, thermocatalytic technologies are substantially unviable as $E_{Thermal} \sim 10^{13}$ GJ yr^{-1} is 100 times the global energy production.

Photocatalysts have an intensity of $E_{Photo} \sim$ 2.1 GJ tonne^{-1} CO_2e (5.3 GJ tonne^{-1} CO_2e GWP100), but could derive this energy directly from solar irradiation [16, 35]. Solar irradiation could also be coupled to electrochemical via photovoltaic (PV) systems where electron–hole harvesting has been optimized for decades. Thus, it could be instructive to compare co-optimized PV with electrocatalysis to photocatalysts. PV-electrocatalytic systems would require a solar energy intensity of $E_{Elec\text{-}PV} \approx E_{Elec}/\eta_{PV} \approx 1$ GJ tonne^{-1} where current commercial PV is $\eta_{PV} \sim 0.2$ [47]. Thus, electrochemical and photochemical have comparable energy intensities when solar powered. Therefore their adoption is likely dictated by other factors such as presence of 'free' forced or natural advection. It is likely that surface coatings on buildings using natural advection can be more easily realized by photocatalysts, whereas internal coatings in ducts may be realized

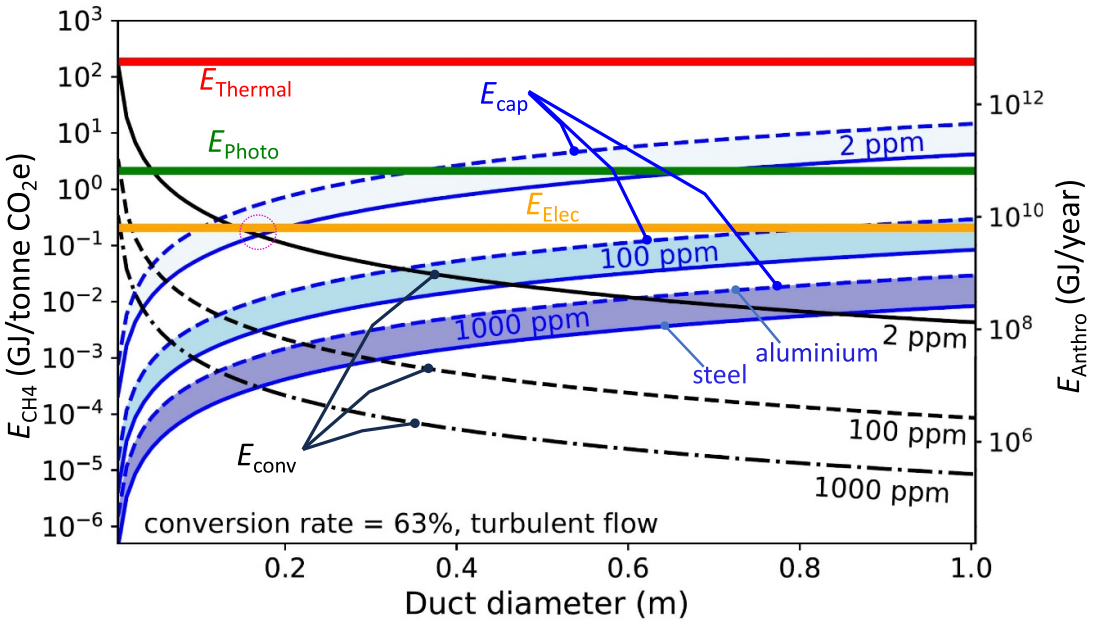

Figure 6. Estimated energy requirements at varying duct diameter, considering a 63% conversion rate in turbulent flow. The values given in the left *y*-axis are scaled by the annual methane emissions, and further considers the 86 times higher global warming potential of methane over CO_2, on a 20 year timescale [1]. The right hand *y*-axis represents the E_{conv} that reflects the annual methane anthropogenic emissions. E_{cap} and E_{conv} are calculated at three different methane concentrations (2 ppm, 100 ppm and 1000 ppm) for aluminium and steel. $E_{Thermal}$ (calculated at 2ppm and 600 K), E_{Photo} and E_{Elec} represent the catalyst input energy of the corresponding optimal catalytic performances.

with PV-electrocatalysts. Finally, this study does not delve into the long-term trajectories of various technologies to make informed comments on research paths over decades, however our analysis highlights that electrochemical catalysts, based on the reviewed information, are most promising compared to photocatalysts and thermal catalysts, as depicted in figure 6.

Abernethy *et al* [48] conducted a study on the viability of methane oxidation technologies, focusing on concentration thresholds and energy efficiency optimization. While their energy intensity metrics, addressing climate and cost neutrality, differ from the ones in the current study, both works highlight the impracticality of heat-based technologies requiring high temperatures for atmospheric methane concentrations. Abernethy *et al* [48] found that achieving cost neutrality at 2 ppm CH_4 in photocatalytic systems necessitates significant advancements in catalytic efficiency, suggesting that using visible wavelengths of light could alleviate concentration constraints. This aligns with the current study's argument that the energy intensity of photocatalysts could directly come from solar irradiation.

5. Environmental evolution of oxidized species

It is important to consider any potential environmental impacts of engineering interventions for methane and the timescales involved. It is well known that methane is an important precursor to tropospheric ozone [49] through the reaction of the methyl peroxy radical (CH_3OO) with nitrogen monoxide (NO) and the subsequent oxidation of CH_3OO to HO_2 and CO_2. The lifetime of the CH_3OO is estimated as only a few seconds, up to a few minutes depending on the concentrations of NO and other reactants [50]. Whilst we lack a full understanding of the likely chemical conditions that would occur under all of the different methane catalysis environments discussed above, following the initial (energy intensive) oxidation step for methane (removal of H-atom), the subsequent radical driven oxidation steps through to the conversion to CO_2 would occur on a time scale of seconds-to-days and could have consequences for the generation of radicals in the vicinity of where the methane oxidation is taking place. An exception in the context of observable presence may be attributed to carbon monoxide with a lifespan of approximately two months [51]. The main implications, however, for global air quality is that a reduction in methane levels will result in a reduction of ozone levels [7].

6. Conclusions

To achieve efficient conversion rates in both atmospheric and source methane abatement systems, it is crucial to consider a broader spectrum of environmental and economic factors. Balancing mass transport and reaction rates is integral to optimizing these systems, where the cost and intensity of processes play

a pivotal role in determining the rate-limiting steps for the technology.

As in any optimized system, the process or species that is expensive (e.g. high financial, energy, or CO_2 intensity) will determine the rate limiting step for the technology. Thus, processes or components that are 'cheap' will be provided in excess to ensure effective use of the expensive process or component. For methane catalysis our analysis shows that for the vast majority of catalytic technologies, the reaction rates limit conversion. Thus, efforts to improve catalytic rates are warranted and can be readily incorporated into systems with sufficiently high molecular fluxes even at atmospheric methane concentrations.

Mass transport of species to the catalyst surface is typically less energy intensive, especially for optimized convective systems paired with photochemical or electrochemical catalysis. This study suggests that optimizing electrocatalytic systems with specific duct configurations can make methane removal more energy-efficient and cost-effective where technologies may be viable at <1 GJ tonne^{-1} CO_2e. Optimized energy intensities were found for advection and ducting material intensity (both $\sim$0.15 GJ tonne^{-1} CO_2e), as well as electrochemical ($\sim$0.2 GJ tonne^{-1}), photochemical ($\sim$2 GJ tonne^{-1}) and thermal ($\sim$180 GJ tonne^{-1}) catalysis. Thus, a total energy intensity for a new installation could be achieved at $\sim$0.5 GJ tonne^{-1}.

Further reductions in energy intensities may be occured if a component of either mass transport or energy input is nominally 'free'. For example, in systems where photon energy is provided freely by the Sun, as in photocatalytic surface coatings on buildings, the primary energy intensities will be associated with the installed photocatalytic material energy intensity. Further, natural advection to the built environment can likely be matched to the catalyst conversion rate by means of optimizing catalyst density within the applied photocatalytic surface coatings. Additional analysis is needed to explore the magnitudes of natural advection to the built environment to accurately determine the magnitude of this potential on a global scale. Likewise, in existing buildings with HVAC ducts where advection already occurs, the additional energy requirement will predominantly be for the electrocatalytic chemical conversion. Collectively, these results show configurations of catalytic methane removal that may prove viable, but significant challenges remain. Efficient methane abatement systems must not only balance mass transport and reaction rates but also strategically prioritize cost-effective and environmentally sustainable components, ensuring optimization for energy efficiency, robustness, safety, cost-effectiveness, and scalability to effectively address climate change.

Data availability statement

All data that support the findings of this study are included within the article (and any supplementary files).

The data produced for this study can be made available upon request to the authors. Please contact A M T at amt83@cam.ac.uk for data inquiries.

Acknowledgment

A M T acknowledges Grantham Foundation for supporting this research.

ORCID iDs

Aliki Marina Tsopelakou https://orcid.org/0009-0009-8981-9429
Adam M Boies https://orcid.org/0000-0003-2915-3273

References

[1] IPCC 2013 *Climate Change 2013: The Physical Science Basis. Contribution of Working Group I to the Fifth Assessment Report of the Intergovernmental Panel on Climate Change* (Cambridge University Press)
[2] Höglund-Isaksson L, Gómez-Sanabria A, Klimont Z, Rafaj P and Schöpp W 2020 Technical potentials and costs for reducing global anthropogenic methane emissions in the 2050 timeframe–results from the gains model *Environ. Res. Commun.* **2** 025004
[3] Jackson R B, Saunois M, Bousquet P, Canadell J G, Poulter B, Stavert A R, Bergamaschi P, Niwa Y, Segers A and Tsuruta A 2020 Increasing anthropogenic methane emissions arise equally from agricultural and fossil fuel sources *Environ. Res. Lett.* **15** 071002
[4] Oeste F D, de Richter R, Ming T and Caillol S 2017 Climate engineering by mimicking natural dust climate control: the iron salt aerosol method *Earth Syst. Dyn.* **8** 1–54
[5] Li Q *et al* 2023 Global environmental implications of atmospheric methane removal through chlorine-mediated chemistry-climate interactions *Nat. Commun.* **14** 4045
[6] Jackson R B *et al* 2021 Atmospheric methane removal: a research agenda *Phil. Trans. R. Soc.* A **379** 20200454
[7] Zosia S, Griffiths P T, Folberth G A, O'Connor Fiona M, Luke A N and Archibald A T 2022 The role of future anthropogenic methane emissions in air quality and climate *NPJ Clim. Atmos. Sci.* **5** 21
[8] Samanta D and Sani R K 2023 Methane oxidation via chemical and biological methods: challenges and solutions *Methane* **2** 279–303
[9] Wang J and He Q P 2023 Methane removal from air: challenges and opportunities *Methane* **2** 404–14
[10] Manion J *et al* 2015 Nist chemical kinetics database, nist standard reference database 17, version 7.0 (web version), release 1.6. 8, data version 2015.09 National Institute of Standards and Technology, Gaithersburg, Maryland, 20899–8320
[11] Chizallet C 2022 Achievements and expectations in the field of computational heterogeneous catalysis in an innovation context *Top. Catal.* **65** 69–81
[12] Stratton S M, Zhang S and Montemore M M 2023 Addressing complexity in catalyst design: from volcanos and

scaling to more sophisticated design strategies *Surf. Sci. Rep.* **78** 100597
[13] Sabatier P 1920 *La Catalyse en Chimie Organique* vol 3 (C. Béranger)
[14] Jiang Y, Fan Y, Li S and Tang Z 2023 Photocatalytic methane conversion: insight into the mechanism of C(sp^3)–H bond activation *CCS Chem.* **5** 30–54
[15] Krogsbøll M, Russell H S and Johnson M S 2023 A high efficiency gas phase photoreactor for eradication of methane from low-concentration sources *Environ. Res. Lett.* **19** 014017
[16] Han B, Wei W, Li M, Sun K and Hu Y H 2019 A thermo-photo hybrid process for steam reforming of methane: highly efficient visible light photocatalysis *Chem. Commun.* **55** 7816–9
[17] Yu L, Shao Y and Li D 2017 Direct combination of hydrogen evolution from water and methane conversion in a photocatalytic system over Pt/TiO_2 *Appl. Catal.* B **204** 216–23
[18] Chen X, Li Y, Pan X, Cortie D, Huang X and Yi Z 2016 Photocatalytic oxidation of methane over silver decorated zinc oxide nanocatalysts *Nat. Commun.* **7** 12273
[19] Luo L, Gong Z, Xu Y, Ma J, Liu H, Xing J and Tang J 2021 Binary Au–Cu reaction sites decorated ZnO for selective methane oxidation to C1 oxygenates with nearly 100% selectivity at room temperature *J. Am. Chem. Soc.* **144** 740–50
[20] Poormohammadi A, Bashirian S, Rahmani A R, Azarian G and Mehri F 2021 Are photocatalytic processes effective for removal of airborne viruses from indoor air? a narrative review *Environ. Sci. Pollut. Res.* **28** 43007–20
[21] Hicks R F, Qi H, Young M L and Lee R G 1990 Structure sensitivity of methane oxidation over platinum and palladium *J. Catal.* **122** 280–94
[22] Wei J and Iglesia E 2004 Reaction pathways and site requirements for the activation and chemical conversion of methane on ru- based catalysts *J. Phys. Chem.* B **108** 7253–62
[23] Wei J and Iglesia E 2004 Mechanism and site requirements for activation and chemical conversion of methane on supported pt clusters and turnover rate comparisons among noble metals *J. Phys. Chem.* B **108** 4094–103
[24] Niwa M, Awano K and Murakami Y 1983 Activity of supported platinum catalysts for methane oxidation *Appl. Catal.* **7** 317–25
[25] Fujimoto K-I, Ribeiro F H, Avalos-Borja M and Iglesia E 1998 Structure and reactivity of Pdo_x/ZrO_2 catalysts for methane oxidation at low temperatures *J. Catal.* **179** 431–42
[26] Ahmad Y H, Mohamed A T, Mahmoud K A, Aljaber A S and Al-Qaradawi S Y 2019 Natural clay-supported palladium catalysts for methane oxidation reaction: effect of alloying *RSC Adv.* **9** 32928–35
[27] Hernandez-Aldave S and Andreoli E 2020 Fundamentals of gas diffusion electrodes and electrolysers for carbon dioxide utilisation: challenges and opportunities *Catalysts* **10** 713
[28] Rocha R S, Camargo L M, Lanza M R V and Bertazzoli R 2010 A feasibility study of the electro-recycling of greenhouse gases: design and characterization of a (TiO_2/RuO_2)/PTFE gas diffusion electrode for the electrosynthesis of methanol from methane *Electrocatalysis* **1** 224–9
[29] Brenneis R J, Johnson E P, Shi W and Plata D L 2021 Atmospheric-and low-level methane abatement via an earth-abundant catalyst *ACS Environ. Au* **2** 223–31
[30] Fan Y, Zhou W, Qiu X, Li H, Jiang Y, Sun Z, Han D, Niu L and Tang Z 2021 Selective photocatalytic oxidation of methane by quantum-sized bismuth vanadate *Nat. Sustain.* **4** 509–15
[31] Yoshida H, Hirao K, Nishimoto J-I, Shimura K, Kato S, Itoh H and Hattori T 2008 Hydrogen production from methane and water on platinum loaded titanium oxide photocatalysts *J. Phys. Chem.* C **112** 5542–51
[32] Jiang Y *et al* 2023 Enabling specific photocatalytic methane oxidation by controlling free radical type *J. Am. Chem. Soc.* **145** 2698–707
[33] Song H, Meng X, Wang S, Zhou W, Song S, Kako T and Ye J 2020 Selective photo-oxidation of methane to methanol with oxygen over dual-cocatalyst-modified titanium dioxide *ACS Catal.* **10** 14318–26
[34] Yuliati L, Itoh H and Yoshida H 2008 Photocatalytic conversion of methane and carbon dioxide over gallium oxide *Chem. Phys. Lett.* **452** 178–82
[35] Hu D, Addad A, Tayeb K B, Ordomsky V V and Khodakov A Y 2023 Thermocatalysis enables photocatalytic oxidation of methane to formic acid at room temperature beyond the selectivity limits *Cell Rep. Phys. Sci.* **4** 101277
[36] Li H, Lei Z, Liu C, Zhang Z and Lu B 2015 Photocatalytic degradation of lignin on synthesized Ag–AgCl/ZnO nanorods under solar light and preliminary trials for methane fermentation *Bioresour. Technol.* **175** 494–501
[37] Song H, Meng X, Wang Z-J, Wang Z, Chen H, Weng Y, Ichihara F, Oshikiri M, Kako T and Ye J 2018 Visible-light-mediated methane activation for steam methane reforming under mild conditions: a case study of Rh/TiO_2 catalysts *ACS Catal.* **8** 7556–65
[38] Lee B and Hibino T 2011 Efficient and selective formation of methanol from methane in a fuel cell-type reactor *J. Catal.* **279** 233–40
[39] Semin G, Belyaev V, Demin A and Sobyanin V 1999 Methane conversion to syngas over pt-based electrode in a solid oxide fuel cell reactor *Appl. Catal.* A **181** 131–7
[40] Park S, Craciun R, Vohs J M and Gorte R J 1999 Direct oxidation of hydrocarbons in a solid oxide fuel cell: I. Methane oxidation *J. Electrochem. Soc.* **146** 3603
[41] Park S, Vohs J M and Gorte R J 2000 Direct oxidation of hydrocarbons in a solid-oxide fuel cell *Nature* **404** 265–7
[42] Tomita A, Nakajima J and Hibino T 2008 Direct oxidation of methane to methanol at low temperature and pressure in an electrochemical fuel cell *Angew. Chem.* **47** 1462–4
[43] Lee B, Sakamoto Y, Hirabayashi D, Suzuki K and Hibino T 2010 Direct oxidation of methane to methanol over proton conductor/metal mixed catalysts *J. Catal.* **271** 195–200
[44] van der Voet E, Salminen R, Eckelman M, Mudd G, Norgate T and Hischier R 2013 *Environmental Risks and Challenges of Anthropogenic Metals Flows and Cycles, A Report of the Working Group on the Global Metal Flows to the International Resource Panel* (UNEP)
[45] Hasanbeigi A, Price L, Chunxia Z, Aden N, Xiuping L and Fangqin S 2014 Comparison of iron and steel production energy use and energy intensity in china and the us *J. Clean. Prod.* **65** 108–19
[46] International Energy Agency 2021 Top twelve emitters of methane with breakdown by sector
[47] Ramasamy V, Zuboy J, O'Shaughnessy E, Feldman D, Desai J, Woodhouse M, Basore P, and Margolis R, Us solar photovoltaic system and energy storage cost benchmarks, with minimum sustainable price analysis: Q1 2022 *Technical Report* (National Renewable Energy Laboratory (NREL))
[48] Abernethy S, Kessler M I and Jackson R B 2023 Assessing the potential benefits of methane oxidation technologies using a concentration-based framework *Environ. Res. Lett.* **18** 094064
[49] Monks P S *et al* 2015 Tropospheric ozone and its precursors from the urban to the global scale from air quality to short-lived climate forcer *Atmos. Chem. Phys.* **15** 8889–973
[50] Wolfe G *et al* 2014 Missing peroxy radical sources within a summertime ponderosa pine forest *Atmos. Chem. Phys.* **14** 4715–32
[51] Forster P *et al* 2007 Changes in atmospheric constituents and in radiative forcing *Climate Change 2007: The Physical Science Basis. Contribution of Working Group I to the 4th Assessment Report of the Intergovernmental Panel on Climate Change*